a reprint from Applied Optics

Characterization of an absolute cryogenic radiometer as a standard detector for radiant-power measurements

R. U. Datla, K. Stock, A. C. Parr, C. C. Hoyt, P. J. Miller, and P. V. Foukal

An active cavity radiometer of the electrical substitution type with a cone receiver that operates at 2–4 K has been developed for measuring radiant fluxes in the dynamic range of 20 nW to 100 μW within an uncertainty of ±1% (2σ level). It is a broadband absolute detector with a flat overall absorption efficiency that is >99% for radiation from the visible to long-wavelength IR. The system is designed based on thermal modeling and experimental measurements of concepts. It has been installed in the cryogenic chamber for low-background infrared radiation calibrations at the National Institute of Standards and Technology (NIST) for testing cryogenic blackbody sources, detectors, and optical components. Its time constant, responsivity, and nonequivalence error have been measured. They are in agreement with design predictions. Radiant power measurements of an amplitude-stabilized He–Ne laser beam with the radiometer and an industry standard photodiode detector, QED-200, have been intercompared and found to be in agreement. The intercomparison ratio of the measurements with the absolute cryogenic radiometer and QED-200 was 1.004 in the 75–100-μW range with an uncertainty of 0.5% (the 3σ level).

Key words: Radiant power, absolute cryogenic radiometer, radiometry, electrical substitution radiometer, visible to long-wavelength IR radiation, photodiode detector intercomparison, low-background IR radiation.

1. Introduction

Absolute cryogenic radiometers (ACR's) are being used increasingly as the standard detectors for absolute radiometry. A review of the historical development of absolute radiometers can be found in Ref. 1. Electrical substitution had been the principal technique for measuring absolute optical power since the original experiments of Kurlbaum and Angstrom nearly a century ago.[1] The technique involves the application of electrical heating to keep the receiver of the radiometer at a constant temperature. When radiation falls on the receiver, to keep the receiver at the same temperature the electrical heater power is reduced by an amount that is equal to the optical power. Therefore the optical power is measured as the difference between the electrical power applied before and after the radiation is permitted to fall on the receiver. In the past two decades cryogenic radiometers have gained acceptance as the primary means for radiometry in standards laboratories because of their improved accuracy.[1,2] A cryogenic radiometer was built at the National Institute of Standards and Technology (NIST) and was used successfully in a liquid helium-cooled cryochamber until early 1985 for measuring the radiant-power output of cryogenic blackbodies.[3] It became unserviceable with age, and a more modern cryogenic radiometer with improved accuracy was built recently for more general calibration and research activity in the IR spectral region of 2–30 μm. A large (60-cm-diameter by 152-cm-long) stainless-steel chamber with its internal copper cryoshield cooled to 20 K by a closed-cycle He refrigerator was built especially to house the radiometer and provide a low-background environment for calibrations and research. The laboratory is called the Low Background Infrared Radiation (LBIR) calibration facility. The physical features and design considerations of the radiometer and the cryochamber are described in recent publications.[3–5] In Sections 2–5 the features of this radiometer are illustrated further from its

R. U. Datla, K. Stock, and A. C. Parr are with the National Institute of Standards and Technology, Gaithersburg, Maryland 20899. C. C. Hoyt, P. J. Miller, and P. V. Foukal are with, Cambridge Research and Instrumentation, Inc., 21 Erie Street, Cambridge, Massachusetts 02139.

Received 27 January 1992.
0003-6935/92/347219-07$05.00/0.

design point of view, and its experimental characterization is described.

Silicon photodiodes have been developed for use as standard detectors.[6] In Section 6 we compare the performance of the NIST LBIR ACR with that of the QED-200 silicon photodiode by measuring the output beam of a He–Ne laser beam at 632.8 nm.

2. NIST LBIR ACR Specifications

The design specifications of this radiometer are an outgrowth of the earlier radiometer at NIST that was operated before 1985. The diameter of the cavity entrance aperture is set to 3.0 cm to maximize the radiative flux collected. A conical cavity with a 45-deg full apex angle is chosen to provide the incident rays at least four reflections inside the cavity to increase the effective absorption of radiation. The receiver can resolve radiative fluxes down to a 0.2-nW level. The sensitivity is limited by only the temperature stabilities of 5 μK rms achieved under feedback control when digital temperature controllers are used. The time constant of the receiver is specified to be as low as possible (i.e., within a few tens of seconds) to have a fast response. The numerical model used to design the ACR with these specifications is described briefly below.

3. Description of the Numerical Model Used to Design the ACR

The thermal response of the cryogenic cavity of the radiometer was modeled with a computer program called the Lumped Parameter Numerical Code. The program used data about the geometry together with temperature-dependent models of the specific heats and conductivities of the various materials. The appropriate heat capacities and thermal impedances are generated as output by the program to describe the radiometer in terms of parameters such as the diameter, the vertex angles, and the thickness of the ACR cone.

The following conditions are used in developing the final design. The receiver is taken to be operated at 2.2 K, which is determined by a pressure-controlled He bath. The He bath is taken to be a fixed-temperature boundary, as is the ambient temperature. The requirement that the receiver resolution be at the 0.2-nW level implied with a 5-μK thermometer noise that the responsivity should exceed 25 K/mW. To achieve this goal, we considered receiver designs of 25-K/mW responsivity.

Finally, we chose the parameters that entered into the design based on our experience at CRI, Inc. constructing cyrogenic receivers and from the results of the lumped parameter numerical code. We also studied the nonequivalence terms by using the lumped parameter model. Figure 1 shows the nodes of principal interest in the model. The temperatures at these nodes are the values shown in tabular columns (a) and (b) in Fig. 1, which were obtained by running the model at 10 μW or electrical heating power and an equal radiative power input, respectively. The key

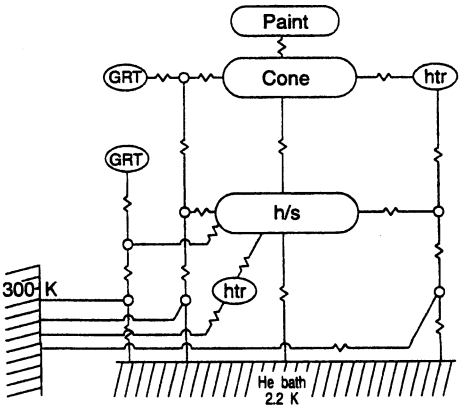

TEMPERATURE (K)

Node	(a) Electrical Heating	(b) Radiative Heating
paint	2.432668	2.432736
cone	2.432668	2.432636
heater windings (htr)	2.432757	2.432601
heat sink (h/s)	2.200284	2.200284
GRT	2.432670	2.432635

Fig. 1. Nodes in the lumped parameter model: GRT's, Ge resistance thermometers.

result from the modeling is that the cavity thermometer and the cone are isothermal to within 1 μK, thus implying a nonequivalence error of $\sim 4.0 \times 10^{-11}$ W, which is negligible in the use of the instrument.

The calculated time behavior of the receiver in response to a 10-μW pulse is illustrated in Fig. 2(a). The predicted time constant to a 50% response is ~22 s. The time constant increases significantly at higher input power. The response to a 100-μW pulse is shown in Fig. 2(b). Figure 3 shows the calculated responsivity (in kelvins per watt) plotted as a function of input power in watts. The responsivity is highest for small signals since the heat-link thermal conductivity drops with temperature. Its peak marginal

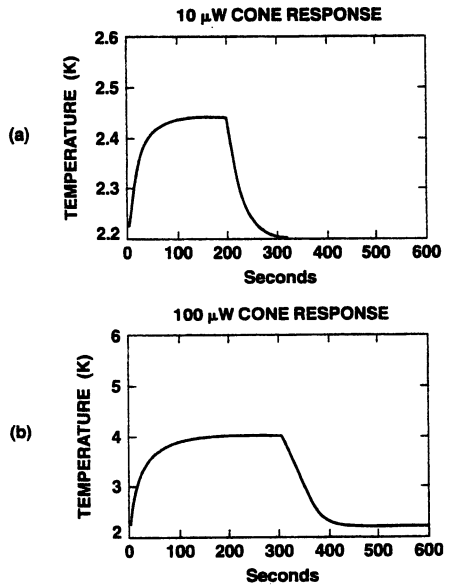

Fig. 2. Calculated response of the ACR receiver for 10- and 100-μW input power.

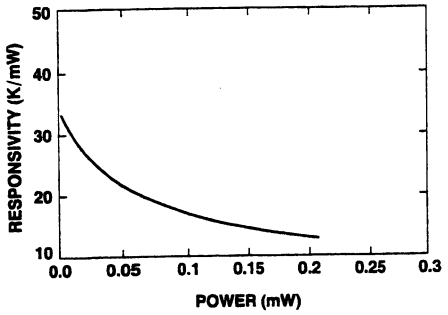

Fig. 3. Calculated responsivity of the ACR receiver.

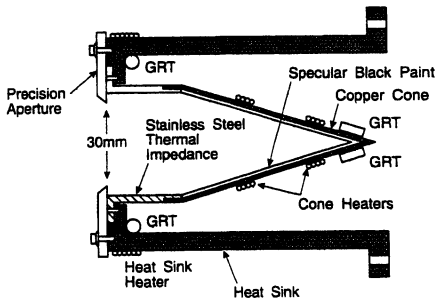

Fig. 5. ACR receiver subassembly.

responsivity is 30 K/mW for input power levels below 10 μW. Figure 4 shows the rising cone temperature with increasing input power. At power levels approaching 1 mW the cone temperature exceeds 8 K and the heater leads will lose their superconducting properties. This and the general drop of responsivity illustrated in Fig. 3 suggest the loss of advantages when this particular cryogenic radiometer for high powers, i.e., powers above 0.1 mW, is used.

4. Physical Description of the ACR Receiver Assembly

Many of the physical features of the ACR have been described in earlier publications.[2,4,5] The receiver subassembly is illustrated in Fig. 5. The receiver cavity is a cone with a 3.2-cm aperture diameter. The inner surface of the cone is coated with specularly reflective black paint. The cavity is constructed of electrodeposited O-free high-conductivity Cu (OFHC) with a 0.127-mm wall thickness. The cylindrical lip is brazed to a stainless-steel tube with a 3.81-cm outer diameter and a 3.04-cm-long and 0.05-mm thick wall, which provides the heat link between the cavity and an OFHC heat sink. Two Ge resistance thermometers (GRT's) are attached symmetrically on the cone outer surface. One is used for measurements, and the other one is a spare. The heat sink is an OFHC tube, the base of which is flange mounted to the back wall of the receiver chamber. The heat-sink temperature is also measured by two GRT's that are located symmetrically as shown in Fig. 5; again one GRT is kept as a spare. The receiver GRT and the heat-sink GRT are monitored by separate temperature controllers located outside the chamber. The GRT's also operate as the temperature sensors of servo loops that control electrical heaters on the receiver and the heat sink. The controllers provide temperature stabilities of 4–5 μK rms at the receiver and heat sink. The menu-driven computer software controls, monitors, and collects the data of power supplied to the heaters.

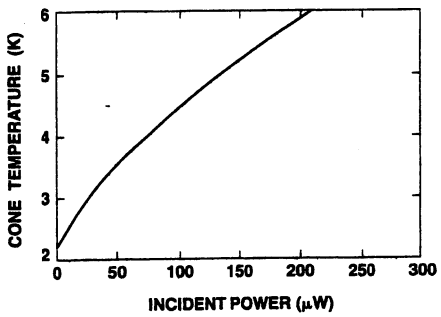

Fig. 4. Variation of the temperature of the ACR receiver cone with incident power.

5. Experimental Characterization of the ACR

The main objective of the characterization is the evaluation of the aspects of the radiometer that affect the overall accuracy, such as aperture area, receiver absorptance, and nonequivalence effects. These effects have been measured, and the results are used to produce an uncertainty budget, which gives the systematic uncertainty of the radiometric measurement.

A. ACR Aperture

The radiometer is designed to provide an extremely accurate measurement of the irradiance at a given distance from a blackbody along the optical axis. An accurately machined 3.0-cm-diam circular aperture made of Invar is mounted on the heat sink as shown in Fig. 5. It is important that the area of the aperture at operating temperatures is known as accurately as possible. Invar (an Fe–Ni alloy, 36 Ni by weight, not to be confused with age-hardenable Invar or zero-crossing Invar) is chosen as the aperture material because it has been shown to have a low-thermal-expansion coefficient throughout the range from 300 to 2 K. The data indicate that the 36% Ni Invar has an average expansion coefficient of $\approx 1 \times 10^{-6}$ between 300 and 0 K.[7]

The determination of the aperture area consists of a measurement of diameter and roundness at room temperature and then an extrapolation of the diameter to operating temperatures based on the thermal expansion data for 36% Ni Invar. Precise measurements of the diameter of the aperture were performed at room temperature by the precision metrology group at NIST. Two different coordinate measuring machines were used. The measured values for the aperture diameter are 29.9573 and 29.9565 mm. Measurements were also made by comparing the diameter of the aperture to a gage block combination. The value that we obtained for the diameter with this method is 29.9584 mm. The average of the three quoted values for the diameter is 29.95740 mm with a standard deviation of 1.17×10^{-4}. The corrected diameter of the aperture at 2.2 K is 29.94212 mm.

The determination of the uncertainty of the aperture area at 4.2 and 2 K was determined with a worst-case analysis. According to the Invar thermal expansion data, the coefficient is always between 0 and 2×10^{-6} and averages $\sim 1 \times 10^{-6}$. The two extreme area changes (zero contraction and 2×10^{-6} linear contraction throughout the temperature range) are 0.05% on either side of the number 7.050 cm^2. Thus the uncertainty assigned to the aperture area at 4.2 and 2 K is 0.05%.

B. Receiver Absorptance

The internal cone surface is coated with a specular carbon black called chemglaze Z302.[8] We characterized the absorptance of this paint by measuring the single reflection at an incidence angle of 45 deg with a spectrophotometer for wavelengths from 0.3 to 40 μm. The results are plotted in Fig. 6. It shows the specular reflectance to be $<10.5\%$ over this wavelength range. Separate tests showed diffuse reflectance to be $<1\%$. The four reflections expected in this 45-deg cone yield a calculated overall absorptance of $>99\%$. A measurement test[5] on the receiver cone at 632.8 nm when an expanded He–Ne laser beam was used showed an absorptance of 99.88 ± 0.1%.

C. Measurements of ACR Parameters

1. *Time Constant*

The time constant of the receiver is measured in a small test chamber where a pulse of 10 μW of heater power is used. A time constant of 18.4 s is observed for a 50% response compared with a calculated value of 22 s. The time constant is not a critical figure of merit for the extended measurements of relatively stable sources. However, the long time constant indicates that the receiver should be permitted to stabilize in response to radiant input after the shutter is opened for at least three time constants before the measurements are started.

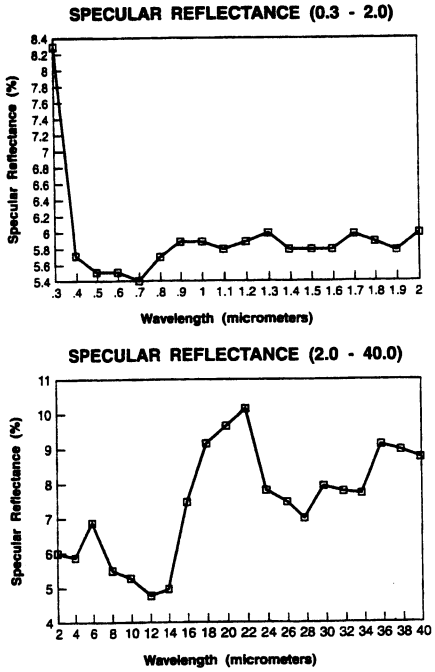

Fig. 6. Absorptance measurements of Chemglaze.

2. *Responsivity*

We measured the responsivity using the following procedure. After we cooled the LBIR chamber to maintain a temperature of 20 K inside by using the closed-cycle He refrigerator system, the radiometer cryostat is filled with liquid He and evacuated to cool the heat sink to a temperature of 2 K. The heat-sink temperature controller is set to maintain a constant temperature at slightly above 2 K by the ac bridge in its active mode controlled by the heat-sink temperature sensor. The temperature sensor is a GRT. The receiver temperature controller is set to operate the receiver in the open mode as a bolometer. A set value of heater power is provided to the receiver by one of its heaters, and the resulting temperature is measured by the receiver temperature sensor (GRT). The heater power is changed to a different value, and the resulting change in the temperature of the receiver is noted. The responsivity is given by

$$\text{responsivity} = (\text{temperature change})/(\text{power change}).$$

The measured value of the responsivity is 29.7 K/mW (±0.1% 1σ) for the receiver operation at ≈2 K.

3. *Measurement of Nonequivalence Error*

The radiometer has been designed to reduce the nonequivalence term to a negligible level. Nonequivalence, such as the difference in the isotherms achieved under electrical and radiative heating and heat losses in the heater leads, has been minimized in the ACR through the use of high-diffusivity Cu and superconducting heater leads made of Nb.

We tested this nonequivalence contribution by sequentially applying a constant electrical power to the two heaters mounted at opposite extremities of the receiver. Equal power inputs should produce equal temperatures at the receiver temperature sensor. If a different temperature results, this difference is an upper limit to the magnitude of the effect present in normal operating conditions. We can translate the temperature difference to a nonequivalence error by dividing the temperature change by the product of the receiver responsivity and power of the heat applied to perform the test. The results of a nonequivalence test are summarized in Table 1.

D. Radiometer Equation and the Uncertainty Budget

The electrical substitution principle is illustrated in Fig. 7. We obtained the flux F falling on the receiver aperture by measuring the equivalent electrical power to maintain the receiver at a constant temperature. The equation to calculate the radiometric power is

$$\text{electrical power} = \text{radiative power},$$

$$V_1(V_2/R) = FAN, \tag{1}$$

Table 1. Nonequivalence Measurement[a]

Receiver Heater	Electrical Power Supplied (μW)	Temperature Measured with the Receiver GRT (K)
Heater 1	0.0	2.3034
	10.0	2.6095
Heater 2	0.0	2.3034
	10.0	2.6094

[a]Nonequivalence = (temperature change)/(responsivity) × (power) × 100 = (0.0001 K)/(29.7 K/mW) × (0.010 mW) × (100) = 0.034%.

where V_1 is the voltage across the heater,
V_2 is the voltage across the current sense resistor,
R is the current sense resistance,
F is the radiant flux,
A is the receiver absorptance, and
N is the nonequivalence.

By solving for the power F, we obtain from Eq. (1)

$$F = V_1(V_2/R)(1/A)(1/N). \quad (2)$$

We determined the total uncertainty of the radiometer characterization by taking into account the uncertainties of individual measurements for each term of Eq. (2). The uncertainty budget is shown in Table 2. The overall systematic uncertainty (bias) is 0.12% (1σ). It is calculated as the square root of the sum of squares (SRSS) of the components listed in Table 2.

E. Measuring the Minimum Sensitivity (Noise Level)

The noise level of the radiometer had to be minimized to achieve a signal-to-noise ratio of 100 for a flux of 20 nW. The ACR is a thermal detector, and the noise level is dependent on the temperature stabilities of the receiver and the heat sink. Thus minimizing the noise level is partially a task of reducing electrical noise in the temperature sensors and optimizing the control parameters. We measured a noise level of 0.2 nW by operating the ACR in a small liquid He-cooled Dewar at 4 K in a controlled experimental setup.

6. Comparison of the ACR Performance with a QED-200 Photodiode

We tested the performance of the ACR by measuring the power of a He–Ne laser beam and intercomparing

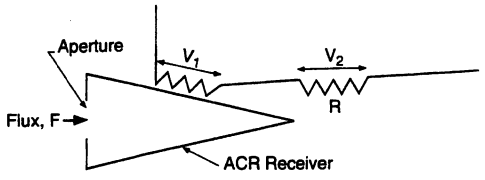

Fig. 7. Electrical substitution principle.

Table 2. Uncertainty Budget for ACR Characterization[a]

Measurement	Method	Magnitude	Uncertainty (1 Standard Deviation of the Mean) (%)
(a) Current sense resistor	NIST calibration ohmmeter	Depends on range	0.01
(b) Voltage	NIST calibration voltmeter	Depends on range	0.05
(c) Receiver absorptance	Integrating sphere at 632.8 nm	(0.9988)	0.1
(d) Nonequivalence	Dual heaters	0.03%	0.03

[a]Total systematic uncertainty given as the SRSS of individual components (a)–(d) (=0.12%).

it with a measurement by using a QED-200 photodiode. A QED-200 has a near-unity quantum efficiency because of the alignment of the three silicon photodiodes in the package in a light-trapping configuration, which results in a near-complete absorption of incident radiation. The ratio of the output current to incident radiation can be calculated on the basis of one electron per incident photon according to the equation.[6]

$$R = \text{wavelength}/1239.5, \quad (3)$$

where R is the responsivity in amperes per watt and the wavelength is in nanometers. It has been established through experiments[6] that the response is near-unity quantum efficiency without an applied bias from 450 to 550 nm. Above 550 nm a bias voltage is necessary to bring the quantum efficiency to near 1 and avoid saturation nonlinearity. In the present experiment the QED-200 detector is checked at 632.8 nm by comparing it with another QED-200 reference standard detector at NIST, and it was adjusted to bring the quantum efficiency to near 1 and eliminate nonlinearity with a 20-V reverse bias for incident radiant powers of 75–100 μW. The upper limit for power measurements with the ACR is 100 μW because of its falling responsivity to higher incident powers, and consequently the intercomparison of the ACR with QED-200 is performed at 75 and 100 μW of incident power from a He–Ne laser.

We obtained the incident He–Ne laser beam power P in watts from the measurement of the QED-200 photocurrent response S in amperes by using Eq. (3) ($P = S/R$). We measured the photocurrent S by converting to voltage by using a transimpedance amplifier. The voltages are measured with a voltmeter. The calibration of the transimpedance of the amplifier circuit yielded a value of 99,896 V/A with an uncertainty of 0.007%. The calibration of the digital voltmeter quoted by the manufacturer and tested at NIST is unity with an uncertainty of 0.014%. The

systematic uncertainty when Eq. (3) is used to characterize a commercial QED response is 0.1% as quoted by the manufacturers based on tests reported in the literature.[6] The total systematic uncertainty is 0.1% for the QED-200 measurements. It is calculated as the SRSS of the three uncertainties.

The experimental setup is shown in Fig. 8. We obtain a beam of vertically polarized light from a He–Ne laser by aligning its polarization with that of a vertical polarizer. The beam was amplitude stabilized by a laser intensity stabilizer.[9] It consisted of an electro-optic modulator [Fig. 8(A)] and a thermally controlled monitor photodiode with a beam splitter [Fig. 8(B)]. These units connected to an electronic servo system stabilized the laser intensity. Long-term fluctuations of laser power are reduced to within 0.05% of output power. The beam is spatially filtered to reduce scattered light. A beam expander, an aperture, and a focusing lens shown in Fig. 8 steered the beam into the receiver cone of the ACR with a spot size of 5 mm. A fused silica glass set at a Brewster angle of 57 deg for vertically polarized light is used as a window at the entrance port to the LBIR chamber to reduce laser power losses caused by reflections. Leakage of the ambient background radiation into the chamber is minimized when nonlimiting apertures are used at the inner and outer cryogenic shields and at a place close to the ACR cone. To simplify the schematic, we do not show the apertures in Fig. 8. Measured values of the background flux levels at the ACR aperture are found to be $< 0.1\%$ of the laser power.

To compare the ACR power measurement with the QED-200, we had to measure the ratio of the laser power outside the LBIR chamber to inside the chamber as a first step in the experiment. We used the QED-200 detector to measure the ratio at the ambient conditions of the temperature and pressure by interchanging its position from outside to inside the chamber and vice versa as shown in Fig. 8. At each position of the QED-200 the beam power is measured for 3 min with a data point recorded every second. We measured the background by blocking the beam with a solid obstruction both before and after the beam power measurements. The background signals are averaged and subtracted from the average signals for beam power measurements. The data are collected for eight such repetitions at various times over several days and for two arbitrarily selected powers of the laser beam, i.e., 75 and 100 μW. The data averages at each power level and the ratios of powers measured internal to the chamber and external to the chamber are shown in Table 3. The uncertainty quoted for each measurement in the table is the SRSS of the systematic (0.1%) and the random components. Column 4 shows the ratios of laser power measured by the QED-200 between its outside-the-chamber and inside-the-chamber positions. The deviation of the ratios from unity is attributed to losses and scatter at the Brewster window. The uncertainty in each ratio is calculated by the propagation of errors from power measurements. As a second step of the experiment the same ratio is measured with the ACR as the detector inside the chamber and the QED-200 as the detector outside the chamber. We cooled the LBIR chamber to 20 K and the radiometer to 2 K to make the measurements. The data are collected every second for 3 min each on the QED-200 and the ACR. We alternated between them using the same laser beam. The background is measured on each device in the same way as described above. The measured values at 75- and 100-μW power levels are shown in Table 4. The quoted uncertainties are the SRSS of the systematic and random components. The systematic uncertainty in the ACR measurement is taken from Table 2, i.e., 0.12%, and the ratios of powers measured by the ACR internal to the chamber and the QED-200 external to

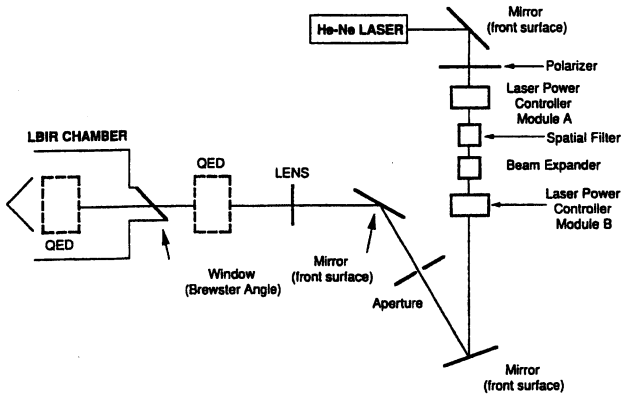

Fig. 8. Experimental setup for the intercomparison of the ACR and QED-200.

Table 3. Comparison of QED-200 Measurements of Laser Power Between Inside and Outside the Chamber

Outside-the-Chamber QED-200 (μW)	Inside-the-Chamber QED-200 (μW)	Ratio(1) QED-200(Outside) / QED-200(Inside)
92.13 ± 0.16	90.56 ± 0.13	1.017 ± 0.002
92.81 ± 0.13	90.79 ± 0.11	1.022 ± 0.002
91.33 ± 0.16	89.58 ± 0.16	1.020 ± 0.003
94.92 ± 0.17	93.05 ± 0.17	1.020 ± 0.003
73.68 ± 0.14	71.93 ± 0.12	1.024 ± 0.003
76.66 ± 0.13	74.93 ± 0.13	1.023 ± 0.003

Weighed mean, 1.021
Standard deviation of the weighed mean, 0.09%

Table 4. Comparison of QED-200 (Outside) and ACR (Inside)

Outside-the-Chamber QED-200 (μW)	Inside-the-Chamber ACR (μW)	Ratio(2) QED-200(Outside) / ACR(Inside)
91.86 ± 0.24	89.51 ± 0.22	1.026 ± 0.004
76.38 ± 0.22	74.56 ± 0.33	1.024 ± 0.005

Weighed mean, 1.025
Standard deviation of the weighed mean, 0.12%

Table 5. Intercomparison of ACR and QED-200

$$\frac{\text{ACR(Inside)}}{\text{QED-200(Inside)}} = \frac{\text{Ratio(2)}}{\text{Ratio(1)}} = 1.004 \pm 0.0015$$

the chamber are shown in the third column of Table 4. Again we calculated the uncertainty in each ratio by the propagation of errors from power measurements. The weighed mean values of the ratios are shown at the bottom of Tables 3 and Table 4. The weight factor is taken to be the inverse square of the standard deviation. Table 5 shows the intercomparison of measurements when the ACR and the QED-200 are used. The ratio is 1.004 with an uncertainty of 0.15% (1σ level).

7. Summary

The ACR used for the measurements of radiation from cryogenic blackbody sources was built to NIST specifications and tested and characterized at the NIST LBIR user facility. We have compared its response with an industry standard solid-state QED-200 by using both devices to measure the beam power from an intensity-stabilized He–Ne laser. The agreement is within 0.5% (a 3σ level).

The authors appreciate the technical support of S. Ebner and J. Proctor in running the experiment. The able assistance of J. Fowler and P. Tobin in the early phase of the LBIR facility is acknowledged.

K. Stock was a visiting scientist from Physikalisch-Technische, Bundesanstalt, Braunschweig, Germany.

References and Notes

1. F. Hengstberger, "The absolute measurement of radiant power," in *Absolute Radiometry: Electrically Calibrated Thermal Detectors of Optical Radiation,* F. Hengstberger, ed. (Academic, San Diego, Calif., 1989), pp. 1–117.
2. P. V. Foukal, C. Hoyt, H. Kochling, and P. Miller, "Cryogenic absolute radiometers as laboratory irradiance standards, remote sensing detectors, and pyroheliometers," Appl. Opt. **29,** 988–993 (1990).
3. C. R. Yokely, "Long wave infrared testing at NBS," in *Applications of Optical Metrology: Techniques and Measurements II,* J. J. Lee, ed., Proc. Soc. Photo-Opt. Instrum. Eng. **416,** 2–7 (1983).
4. A. C. Parr, J. Fowler, and S. Ebner, "Low background infrared calibration facility at the National Bureau of Standards," in *Infrared Scene Simulation: Systems, Requirements, Calibration, Devices, and Modeling,* R. B. Johnson and M. J. Triplett, eds., Proc. Soc. Photo-Opt. Instrum. Eng. **940,** 26–33 (1988).
5. S. C. Ebner, A. C. Parr, and C. C. Hoyt, "Update on the low background IR calibration facility at the National Institute of Standards and Technology," in *Imaging Infrared: Scene Simulations, Modeling, and Real Image Tracking,* A. J. Huber, M. J. Triplett, and J. R. Wolverton, eds., Proc. Soc. Photo-Opt. Instrum. Eng. **1110,** 49–60 (1989).
6. E. F. Zalewski and C. R. Duda, "Silicon photodiode device with 100% external quantum efficiency," Appl. Opt. **22,** 2867–2873 (1983).
7. A. F. Clark, "Thermal expansion," in *Materials at Low Temperatures,* P. R. Reed and A. F. Clark, eds. (American Society for Metals, Metals Park, Ohio, 1983), pp. 75–128.
8. Product of Lord Corporation, Industrial Coatings Division, 2000 West Grandview Boulevard, Erie, Pa. 16514-0038.
9. Laser Power Controller system, Models LPC-VIS and RD-40, manufactured by Cambridge Research and Instrumentation, Inc., 21 Erie Street, Cambridge, Mass. 02139.